Silicon Nanoparticles as Hyperpolarized Magnetic Resonance Imaging Agents

Jacob W. Aptekar,[†,▽] Maja C. Cassidy,[†,▽] Alexander C. Johnson,[†] Robert A. Barton,[†] Menyoung Lee,[†] Alexander C. Ogier,[†] Chinh Vo,[†] Melis N. Anahtar,[‡] Yin Ren,[‡] Sangeeta N. Bhatia,[‡,§,⊥] Chandrasekhar Ramanathan,[¶] David G. Cory,[¶] Alison L. Hill,[#] Ross W. Mair,[#] Matthew S. Rosen,[†,#] Ronald L. Walsworth,[†,#] and Charles M. Marcus[†,*]

[†]Department of Physics, Harvard University, Cambridge, Massachusetts 02138, [‡]Harvard—MIT Division of Health Sciences and Technology, Massachusetts Institute of Technology E19-502D Cambridge, Massachusetts 02139, [§]Electrical Engineering and Computer Science, Massachusetts Institute of Technology, Cambridge, Massachusetts 02139, [⊥]Division of Medicine, Brigham and Women's Hospital, Boston, Massachusetts 02115, [¶]Department of Nuclear Science and Engineering, Massachusetts Institute of Technology, Cambridge, Massachusetts 02139, and [#]Harvard—Smithsonian Center for Astrophysics, 60 Garden Street, MS 59, Cambridge, Massachusetts 02138. [▽]These authors contributed equally to this work.

ABSTRACT Magnetic resonance imaging of hyperpolarized nuclei provides high image contrast with little or no background signal. To date, *in vivo* applications of prehyperpolarized materials have been limited by relatively short nuclear spin relaxation times. Here, we investigate silicon nanoparticles as a new type of hyperpolarized magnetic resonance imaging agent. Nuclear spin relaxation times for a variety of Si nanoparticles are found to be remarkably long, ranging from many minutes to hours at room temperature, allowing hyperpolarized nanoparticles to be transported, administered, and imaged on practical time scales. Additionally, we demonstrate that Si nanoparticles can be surface functionalized using techniques common to other biologically targeted nanoparticle systems. These results suggest that Si nanoparticles can be used as a targetable, hyperpolarized magnetic resonance imaging agent with a large range of potential applications.

KEYWORDS: silicon nanoparticle · contrast agent · hyperpolarized · molecular imaging · functionalized nanoparticle · magnetic resonance imaging (MRI) · nuclear magnetic resonance · nuclear spin relaxation

The use of nanoparticles for biomedical applications has benefited from rapid progress in nanoscale synthesis of materials with specific optical[1−3] and magnetic properties,[4] as well as biofunctionalization of surfaces, allowing targeting,[5−7] *in vivo* tracking,[1,7,8] and therapeutic action.[3,9] Porous silicon nanostructured materials are of interest for molecular and cell-based biosensing, drug delivery, and tissue engineering applications.[10,11] For magnetic resonance imaging (MRI), superparamagnetic nanoparticles have extended susceptibility-based contrast agents toward targeted imaging,[4] though achieving high spatial resolution with high contrast remains challenging, especially in regions with natural magnetic susceptibility gradients. An alternative approach is direct MRI of hyperpolarized materials with little or no background signal. Hyperpolarized noble gases[12−14] and ^{13}C-enhanced biomolecules[15,16] have demonstrated impressive image contrast, but are limited by short *in vivo* enhancement times (∼10 s for noble gases,[12] ∼30 s for ^{13}C biomolecules[15,16]).

Nuclear magnetic resonance (NMR) in silicon has been widely investigated for half a century[17] and with renewed interest recently in the context of quantum computation.[19] It is known that bulk silicon can exhibit multihour nuclear spin relaxation (T_1) times at room temperature[17] and can be hyperpolarized *via* dynamic nuclear polarization (DNP).[18] The low natural abundance of spin-$^1/_2$ ^{29}Si nuclei (4.7%) embedded in a lattice of zero-spin ^{28}Si nuclei isolates the active nuclear spins from one another and from the environment, leading not only to long T_1 times, but also decoherence (T_2) times of up to tens of seconds.[19] Moreover, the weak dipole−dipole coupling of the sparse ^{29}Si atoms, together with the isotropic crystal structure and the absence of nuclear electric quadrupole moment conspire to keep any induced nuclear polarization aligned with even very weak external fields as the nanoparticle tumbles in space, which occurs, for instance, in fluid suspensions.

This paper investigates in detail two critical properties of Si nanoparticles for their use as targetable hyperpolarized MRI imaging agents. First, we demonstrate for the first time that Si nanoparticles retain long T_1 times at room temperature into the submicrometer regime, and investigate how T_1 depends on size for a variety of commercial and ball-milled Si nanoparticles. This dependence is compared to a model of nuclear spin

*Address correspondence to marcus@harvard.edu.

Received for review August 12, 2009 and accepted November 17, 2009.

Published online December 1, 2009.
10.1021/nn900996p

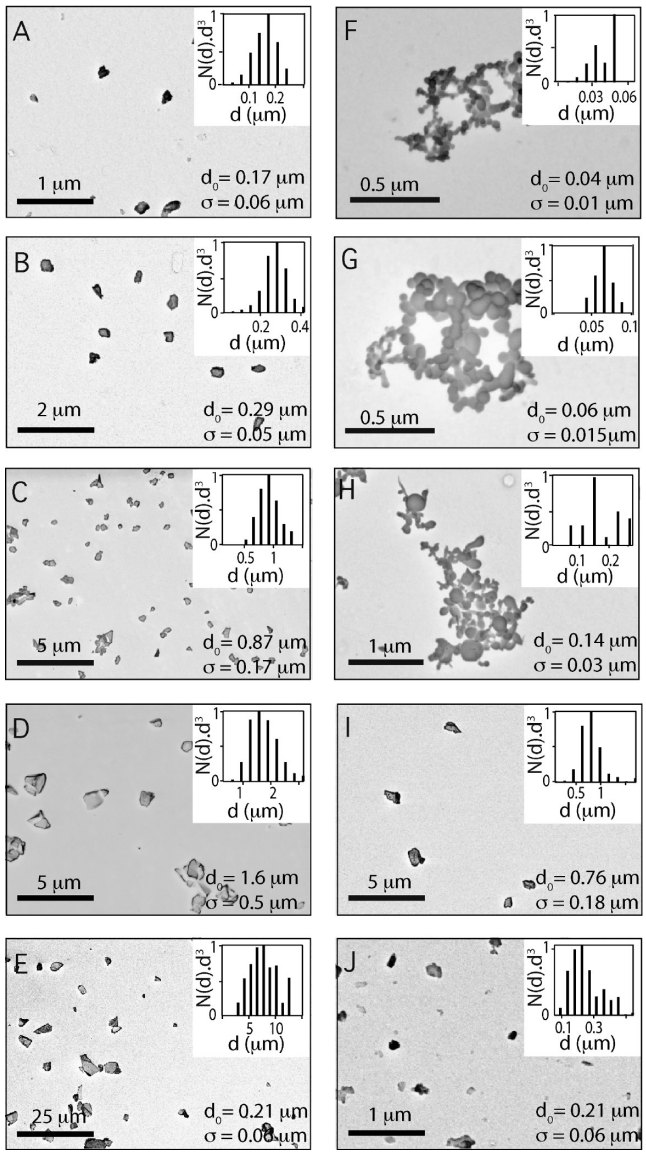

Figure 1. Sizes and shapes of silicon particles. Electron micrographs of Si nanoparticles (A−E) ball milling high-resistivity silicon wafer, (F−G) wet synthesis (Meliorum), (H) plasma synthesis (MTI), (I) electrical explosion (NanoAmor), and (J) ball milling low-resistivity wafer. Insets: Volume-weighted histograms of diameters following size segregation along with averages d_0 and standard deviations σ based on Gaussian fits to distributions.

diffusion,[18] yielding reasonable consistency between theory and experiment. Second, we demonstrate that long-T_1 Si nanoparticles can be surface functionalized by methods similar to those used to prepare other targeted nanoparticle systems.[20,21]

RESULTS

Particle Characterization. Particle size determines regimes of application to biomedicine[22] as well as NMR properties.[18] We investigated room-temperature NMR properties of Si particles spanning four orders of magnitude in mean diameter, from 40 nm to 1 mm. Particles were made by various methods, including ball-milling of nominally undoped (high-resistivity 30−100 kΩ-cm) and highly doped (low-resisitivity 0.01−0.02 Ω-cm) commercial silicon wafers, followed by segregation by size (see Methods). We also investigated chemically synthesized Si nanoparticles with mean diameters 40 nm (wet synthesis, 99.99% elemental purity, Meliorum Corp.), 60 nm (wet synthesis, 99.99% elemental purity, Meliorum Corp.), 140 nm (plasma synthesis, 99% elemental purity, MTI Corp.), and 600 nm (electrical explosion synthesis, 98% elemental purity, Nanostructured & Amorphous Materials, Inc.), obtained commercially. Figure 1 shows representative scanning electron microscope (SEM) images of all measured particles, along with volume-weighted size distributions obtained by SEM image analysis.

^{29}Si NMR Measurements. Nuclear T_1 times of dry Si nanoparticles were measured at room temperature at a magnetic field of 2.9 T using a saturation-recovery NMR pulse sequence with repeated spin−echoes for signal enhancement (see Methods). Values for T_1 are extracted from exponential fits, $A \propto 1 - \exp(-\tau_{pol}/T_1)$, to the Fourier amplitude, A, of the free induction decay (FID) and echoes as a function of polarization time, τ_{pol} (see Figure 2, inset). Figure 2 shows T_1 as a function of volume-weighted average particle diameter for the various samples, as well as a shell−core nuclear spin diffusion model,[18] which has no free parameters. The model assumes T_1 is determined by nuclear spin diffusion to the particle surface, where nuclear spin is quickly relaxed. Undoped ball-milled samples follow a roughly linear dependence on size, $T_1 \propto d_0$, for $d_0 < \sim 10$ μm, saturating at $T_1 \sim 5$ h for larger particles. The trend of increasing T_1 in larger particles is qualitatively consistent with the shell−core model, and suggests that T_1 is governed by surface relaxation. Electron spin resonance (ESR) measurements (see Supporting Information S1) show a single peak corresponding to a g-factor of $g = 2.006$, characteristic of P_b-type defect centers at the Si−SiO_2 interface.[23] The shift toward lower T_1 compared to the core−shell model presumably reflects relaxation within the core, which can be attributed to defects and strain induced either by ball milling[24] or noncrystallinity, depending on the method of synthesis. The highly doped ball-milled particles have $T_1 \approx 200$ s, independent of size. Here T_1 is shortened due to relaxation by free carriers. Smaller commercial particles formed by wet synthesis (>99.99% elemental purity, Meliorum) and plasma synthesis (>99% elemental purity, MTI) have T_1 times as long as 700 s, exceeding the predictions of the core−shell model. Larger commercial particles formed by electrical explosion (>98% elemental purity, NanoAmor) have shorter T_1 than the comparably sized high-resistivity ball-milled particles.

We have also measured the inhomogeneous dephasing times, T_2^*, as a function of mean particle diameter for undoped ball-milled samples at 4.7 T (using a Bruker DMX-200 NMR console). T_2^* ranges from 0.3 ms for $d_0 \sim 0.2$ μm to 1.8 ms for for $d_0 \sim 1000$ μm. We note that while T_1 changes by two orders of magni-

tude over the range of measured particle sizes, T_2^* changes only by a factor of ~6.

MRI of Hyperpolarized Si Nanoparticles. A first demonstration of imaging hyperpolarized Si nanoparticles is shown in Figure 3. A phantom in the shape of the letter H was filled with undoped ball-milled particles (d_0 = 1.6 μm) and allowed to equilibrate at low temperature (4.2 K) and high field (5 T) for 60 h,[15] which enhanced the nuclear spin polarization a factor of ~16 compared to room-temperature polarization at that field. The sample was then removed and imaged at room temperature at 4.7 T (using a Bruker DMX-200 spectrometer with a microimaging gradient set). The transfer from the low temperature environment to the imager required ~60 s, much shorter than the T_1 of the nanoparticles. The phantom was imaged using a small-tip-angle gradient-echo sequence[25] with the following parameters: tip angle θ = 9°, echo time τ = 1.2 ms, field of view = 15 mm, sample thickness = 2.5 cm, single pass (no averaging), acquisition time = 11 s. The resulting image is shown in Figure 3B. MRI of the same sample equilibrated in the field of the imager at room temperature yielded no detectable image.

Surface Functionalization. To examine the applicability of Si nanoparticles to targeted MRI, we prepared the Si nanoparticle surface for attachment to biological-targeting ligands. Nanoparticles were aminated using either (3-aminopropyl)triethoxysilane (APTES) or a 1:2 mixture by volume of APTES with bis-(triethoxysilyl)ethane (BTEOSE) or (3-trihydroxysilyl)propyl methylphosphonate (THPMP) (see Figure 4A and Methods).[26] Results are shown for ball-milled high resistivity nanoparticles (d_0 = 200 nm). Successful amination was assessed using fluorescence spectroscopy (Figure 4B). The high level of fluorescence observed for aminated particles results from the covalent bonding of surface amino groups with fluorescamine, showing these functional groups were accessible for further reaction.

In addition to chemical assays, the accumulation of amines was indirectly monitored by measuring the surface charge of the particles in solution, or zeta potential (ζ)[27] (Figure 4C). The surface of the unmodified silicon nanoparticles is composed of hydroxyl groups from the silicon dioxide and thus shows a negative zeta potential. Particles treated with APTES have surfaces coated with propylamines, which become protonated and positively charged in acidic solutions and show a positive zeta potential.[27]

Aminated particles were coated with polyethylene glycol (PEG) polymers to confer stability and biocompatibility. PEG coating of silica and iron-oxide nanoparticles has been shown to be nontoxic[28] and to reduce the rate of clearance by organs such as the liver

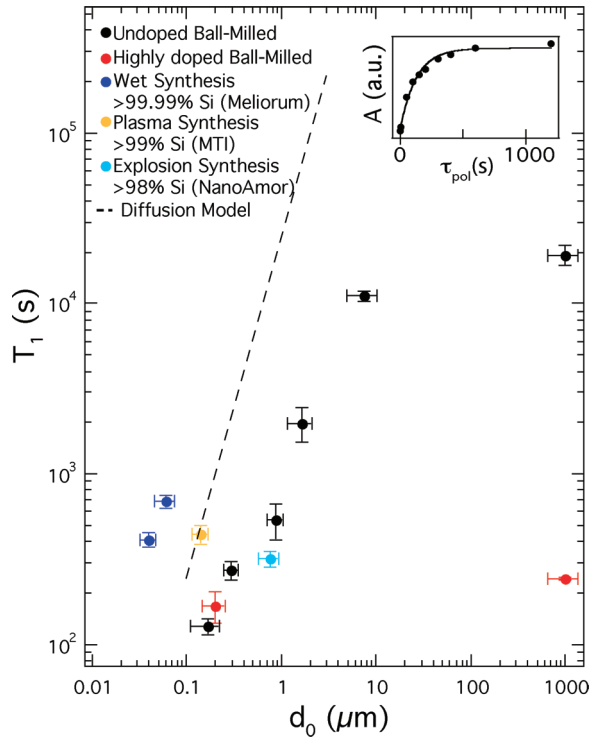

Figure 2. NMR Properties of Silicon Particles. Nuclear spin relaxation (T_1) times at 2.9 T as a function of particle diameter d_0 for various Si particles. Vertical error bars are from exponential fits to relaxation data; horizontal error bars are σ of size distributions (see Figure 1). Inset: Fourier-transform NMR peak amplitude, A, as a function of polarization time τ_{pol} (see text) for the ball-milled high-resistivity particles with d_0 = 0.17 μm. T_1 values were measured using a saturation recovery spin echo pulse sequence described in the text.

or kidneys, thus increasing the particle's circulation time *in vivo*.[28] Pegylation was performed with either α-methyl-PEG-succinimidyl α-methylbutanoate (mPEG-SMB) (Nektar) or maleimide-PEG-*N*-hydroxysuccinimide (MAL-PEG-NHS) (Nektar) (see Methods section). Both SMB and NHS are reactive with amines on the particle surface. The stability of nanoparticles in solution was assessed using both dynamic light scattering (DLS) (Nano ZS90, Malvern) as a measure of the particles' hydrody-

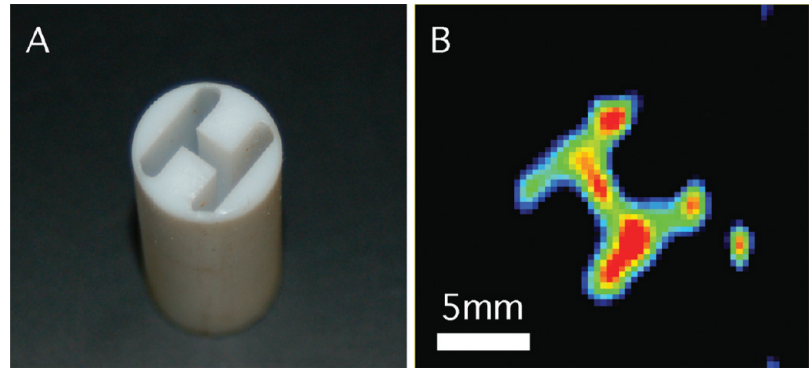

Figure 3. ^{29}Si Magnetic resonance imaging of hyperpolarized Si nanoparticles. (A) An H-shaped phantom filled with high-resistivity Si particles (d_0 = 1.6 μm) prepolarized at low temperature (T = 4.2 K) and high magnetic field (B = 5 T) for 60 h and warmed and transferred to a 4.7 T imager. (B) Single ^{29}Si image of phantom in panel A. See text for imaging details. No ^{29}Si image could be obtained without hyperpolarization using the same sequence.

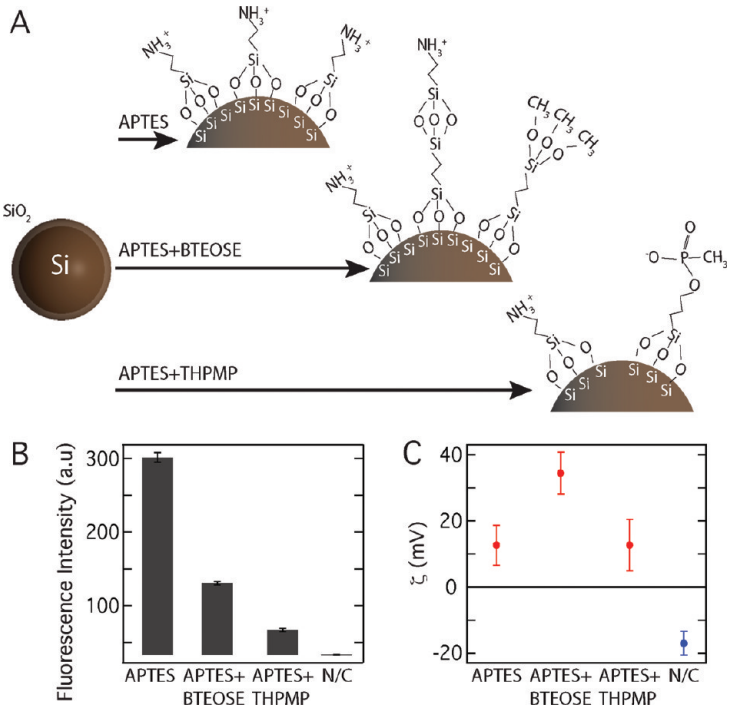

Figure 4. Biological surface modification of silicon nanoparticles. (A) Silicon particles (d_0 = 0.2 μm) were aminated using either (3-aminopropyl)triethoxysilane (APTES) alone or as a 1:2 mixture by volume of APTES with bis-(triethoxysilyl)ethane (BTEOSE) or (3-trihydroxysilyl)propyl methylphosphonate (THPMP in H_2O). (B) Fluorescence spectroscopy confirmed the success of the amination reaction. No fluorescence was evident with the negative control (N/C). (C) A change in the sign of the surface charge, or zeta potential of the particles was evident after amination with the three amine groups (red) when compared to the negative control (blue).

namic radius, and visual determination of flocculation and sedimentation. The particles treated with mPEG-SMB and NHS-PEG-MAL were both stable in phosphate-buffered saline (PBS) for a period of two days with no significant change in the hydrodynamic radius (see Supporting Information, S2). As a control, mPEG−amine polymer, which does not contain amine-reactive groups, was used. The aminated particles treated with mPEG−amine aggregated after centrifugation and resuspension in PBS. These results are consistent with other reports of the successful pegylation of SiO_2 nanoparticles.[29,30]

DISCUSSION

We have demonstrated several key features of Si nanoparticles that establish their potential as a hyperpolarized imaging agent for MRI, including long nuclear relaxation times and receptivity to surface modification with biologically compatible ligands. Room temperature nuclear relaxation (T_1) times for all measured particles were found to be considerably longer than those of previously reported hyperpolarized MRI imaging agents,[12,14−16] in the range of tens of minutes to hours. Moreover, T_1 in the Si system can be tuned by size and doping, allowing optimization for specific applications in biomedical imaging. We examined T_1 as a function of diameter for particles made by ball-milling undoped silicon wafers as well as chemically synthesized nanoparticles. Preliminary measurements on other surface-functionalized silicon nanoparticles[31] indicate that the functionalization process does not reduce the nuclear T_1 of the particles. MRI of Si nanoparticles was demonstrated at modestly enhanced polarization using low-temperature equilibration. While these polarizations are presumably too small for practical use, the results demonstrate that nanoparticles can be successfully transported through large magnetic and temperature gradients without a significant loss of an enhanced polarization. Significantly higher nuclear polarizations (exceeding 10^4 times room-temperature equilibrium polarization at 3*T*) are expected using DNP, with corresponding improvements in image resolution and contrast.[12−16] Optimizing DNP to achieve high polarization will be the subject of future work. The demonstrated coatings with APTES and PEG are important steps for further surface functionalization and, ultimately, biological targeting. In conclusion, the data presented here are necessary for establishing the utility of Si nanoparticles as a flexible platform for imaging agents in MRI.

METHODS

Nanoparticle Preparation and Size Separation. Nominally undoped float-zone grown Si wafers (Silicon Quest International) were ⟨111⟩ oriented, with residual p-dopants and nominal resistivity 30−100 kΩ-cm, depending on batch. Highly doped wafers (Virginia Semiconductor) were Czochralski grown, ⟨100⟩ oriented, boron-doped (p-type), with nominal resistivity 0.01−0.02 Ω-cm.

Ball-milled particles were processed as follows. Whole wafers were shattered using a mortar and pestle. Batches of 8.5 g wafer shards were dry ground for 10 min at 400 rpm in a planetary ball mill (Retsch PM100) using 10 1-cm diameter zirconia balls. The resulting powder was mixed with 20 mL of ethanol and milled under similar conditions for another 3.8 h. For a final milling, also at 400 rpm, 50 3-mm diameter zirconia balls were used. The slurry was milled for times ranging from 1 to 26 h, to give an approximately uniform size distribution between 100 nm and 1 μm. The ball-milled silicon nanoparticles in ethanol were separated by size using a centrifugational sedimentation process. Parameters were calculated using the Stokes equation.[34] From repeated sonication and centrifugal separation, a number of discrete particle size groups could be obtained.

Scanning Electron Microscopy and Size Characterization. Scannning electron microscopy and particle-measuring software (Gatan Digital Micrograph) were used to determine the size distributions of the nanoparticles. Dilute suspensions of silicon nanoparticles in ethanol were sonicated for 10 mins before being pipetted onto a vitreous carbon planchett which was mounted on a standard specimen holder with conducting carbon tape. An acceleration voltage of 2 kV was used. For each sample, >1000 particles were analyzed, sourced from ~50 images. Particle agglomeration seen in dry Meliorum and MTI samples has been reported in similarly sized silica nanoparticles,[29] but is not expected to occur after pegylation. In these cases (Meliorum, MTI), individual measurement of the particle diameter from SEM images was used instead of software analysis.

T_1 Measurements. Nuclear T_1 times of the Si nanoparticles, segregated by size and packed dry in Teflon NMR tubes, were measured at room temperature at a magnetic field of 2.9 T using a spin−echo Fourier transform method with a saturation recovery sequence. Following a train of 16 hard $\pi/2$ pulses to null any initial polarization, the sample was left at field to polarize for a time τ_{pol}, followed by a Carr−Purcell−Meiboom−Gill (CPMG) sequence $(\pi/2)_X - [\tau - (\pi)_Y - \tau -$ echo $]^n$ with $\tau = 0.5$ ms and $n = 200$. In Si and other nuclear-dipole-coupled materials echo sequences can yield anomalously long decay tails.[33] However, the Fourier amplitude of the echo train still provides a signal proportional to initial polarization.[33] Values for T_1 are extracted from exponential fits, $A \propto 1 - \exp(-\tau_{pol}/T_1)$, to the amplitude, A, of Fourier transform of the echo train for 200 echoes as a function of polarization time (see Figure 2a, inset for an example).

Amination. Amination was performed using either (3-aminopropyl)triethoxysilane (APTES, Sigma, 99%) alone or as a 1:2 mixture by volume of APTES with bis-(triethoxysilyl)ethane (BTEOSE, Aldrich, 96%) or (3-trihydroxysilyl)propyl methylphosphonate (THPMP, Aldrich, 42 wt % in H_2O). The surface oxide was first etched with a dilute solution of hydrofluoric acid (8% in ethanol) followed by resuspension of the particles in ethanol. Approximately 100 mg of silicon nanoparticles were added to 45 mL of acidified 70% ethanol (0.04% v/v, adjusted to pH 3.5 with HCl) or methanol buffer (0.1 mM $NaHCO_3$ in methanol), and the solution was placed in an ultrasonic bath for 5 mins. Saline (0.10−0.15 M) was then added and the solution was shaken for 18−24 h. Silanes were removed from the nanoparticle solution by washing and resuspending three times in methanol buffer, with the final resuspension performed with 10 mL of ethanol or methanol buffer.

Fluorescamine Assay. The concentrations of all of the particles were equalized by adjusting their absorption at 420 nm using a spectrophotometer (SpectraMax Plus, Molecular Devices). The fluorescamine reagent was prepared by dissolving 3.5 mg of fluorescamine (Sigma) in 1 mL of dimethyl sulfoxide (DMSO). Within a 96-well standard opaque tray, 10 μL of the fluorescamine solution were added simultaneously to each well containing 40 μL of nanoparticles and mixed thoroughly for 1 min. Fluorescence was measured using an excitation at 390 nm and emission at 465 nm (SpectraMax Gemini XPS, Molecular Devices).

Pegylation. A 10 mg portion of PEG was mixed in 500 μL of methanol buffer and heated briefly at 50 °C to dissolve. Approximately 0.1 mg of aminated particles (100 μL in solution) were added to this solution and it was placed in an ultrasonic bath for 1−3 h. To remove the unreacted PEG, samples were centrifuged and resuspended twice in methanol and finally in a phosphate-buffered saline solution (PBS, 0.1 M Na_2HPO_4, 0.015 M NaCl buffer).

Acknowledgment. We thank D. C. Bell, F. Kuemmeth, T. F. Kosar, C. Lara, D. Reeves, S. Rodriques, and J. R. Williams for technical contributions and D. J. Reilly, C. Farrar, and B. Rosen for valuable discussions. This work was supported by the NIH under grant R21 EB007486-01A1, U54 CA119335, R01 CA124427 and by the NSF through the Harvard NSEC. Part of this work was performed at the Harvard Center for Nanoscale Systems (CNS), a member of the National Nanotechnology Infrastructure Network (NNIN), which is supported by the National Science Foundation under NSF award no. ECS-0335765.

Supporting Information Available: Electron spin resonance measurements, particle stability following PEGylation. This material is available free of charge *via* the Internet at http://pubs.acs.org.

REFERENCES AND NOTES

1. Gao, X.; Cui, Y.; Levenson, R. M.; Chung, L. W. K.; Nie, S. *In-Vivo* Cancer Targeting and Imaging with Semiconductor Quantum Dots. *Nat. Biotechnol.* **2004**, *22*, 969–976.
2. Liu, W.; Howarth, M.; Greytak, A. B.; Zheng, Y.; Nocera, D. G.; Ting, A. Y.; Bawendi, M. G. Compact Biocompatible Quantum Dots Functionalized for Cellular Imaging. *J. Am. Chem. Soc.* **2008**, *130*, 1274–1284.
3. Hirsch, L. R.; Stafford, R. J.; Bankson, J. A.; Sershen, S. R.; Rivera, B.; Price, R. E.; Hazle, J. D.; Halas, N. J.; West, J. L. Nanoshell-Mediated Near-Infrared Thermal Therapy of Tumors under Magnetic Resonance Guidance. *Proc. Nat. Acad. Sci. U.S.A.* **2003**, *100*, 13549–13554.
4. Weissleder, R.; Elizondo, G.; Wittenberg, J.; Rabito, C. A.; Bengele, H. H.; Josephson, L. Ultrasmall Superparamagnetic Iron Oxide: Characterization of a New Class of Contrast Agents for MR Imaging. *Radiology* **1990**, *175*, 489–493.
5. Atanasijevic, T.; Shusteff, M.; Fam, P.; Jasanoff, A. Calcium-Sensitive MRI Contrast Agents Based on Superparamagnetic Iron Oxide Nanoparticles and Calmodulin. *Proc. Natl. Acad. Sci. U.S.A.* **2006**, *103*, 14707–14712.
6. Akerman, M. E.; Chan, W. C. W.; Laakkonen, P.; Bhatia, S. N.; Ruoslahti, E. Nanocrystal Targeting *In-Vivo*. *Proc. Natl. Acad. Sci. U.S.A.* **2002**, *99*, 12617–12621.
7. Weissleder, R.; Kelly, K.; Sun, E. Y.; Shtatland, T.; Josephson, L. Cell-Specific Targeting of Nanoparticles by Multivalent Attachment of Small Molecules. *Nat. Biotechnol.* **2005**, *23*, 1418–1423.
8. Högemann, D.; Ntziachristos, V.; Josephson, L.; Weissleder, R. High Throughput Magnetic Resonance Imaging for Evaluating Targeted Nanoparticle Probes. *Bioconjugate Chem.* **2002**, *13*, 116–121.
9. Simberg, D.; Duza, T.; Park, J. H.; Essler, M.; Pilch, J.; Zhang, L.; Derfus, A. M.; Yang, M.; Hoffman, R. M.; Bhatia, S. N.; *et al*. Biomimetic Amplification of Nanoparticle Homing to Tumors. *Proc. Natl. Acad. Sci. U.S.A.* **2007**, *104*, 932–936.
10. Tasciotti, E.; Liu, X.; Bhavane, R.; Plant, K.; Leonard, A.; Price, B. K.; Cheng, M. M.-C.; Decuzzi, P.; Tour, J. M.; Robertson, F.; Ferrari, M. Mesoporous Silicon Particles as a Multistage Delivery System for Imaging and Therapeutic Applications. *Nat. Nanotechnol.* **2008**, *3*, 151–157.
11. Park, J. H.; Gu, L.; von Maltzahn, G.; Ruoslahti, E.; Bhatia, S. N.; Sailor, M. J. Biodegradable luminescent porous silicon nanoparticles for *in-vivo* applications. *Nat. Mater.* **2009**, *8*, 331–336.
12. Leawoods, J. C.; Yablonskiy, D. A.; Saam, B.; Gierada, D. S.; Conradi, M. S. Hyperpolarized He-3 gas production and MR Imaging of the Lung. *Concepts Magn. Reson.* **2001**, *13*, 277–293.
13. Schröder, L.; Lowery, T. J.; Hilty, C.; Wemmer, D. E.; Pines, A. Molecular Imaging Using a Targeted Magnetic Resonance Hyperpolarized Biosensor. *Science* **2006**, *314*, 446–449.
14. Patz, S.; Muradian, I.; Hrovat, M. I.; Ruset, I. C.; Topulos, G.; Covrig, S. D.; Frederick, E.; Hatabu, H.; Hersman, F. W.; Butler, J. P. Human Pulmonary Imaging and Spectroscopy with Hyperpolarized Xe-129 at 0.2 T. *Acad. Radiol.* **2008**, *15*, 713–727.
15. Golman, K.; Olsson, L. E.; Axelsson, O.; Mansson, S.; Karlsson, M.; Petersson, J. S. Molecular Imaging Using Hyperpolarized 13C. *Br. J. Radiol.* **2003**, *76*, 118–127.
16. Nelson, S. J.; Vigneron, D.; Kurhanewicz, J.; Chen, A.; Bok, R.; Hurd, R. DNP-Hyperpolarized C-13 Magnetic Resonance Metabolic Imaging for Cancer Applications. *Appl. Magn. Reson.* **2008**, *34*, 533–544.
17. Shulman, R. G.; Wyluda, B. J. Nuclear Magnetic Resonance of Si29 in n- and p-Type Silicon. *Phys. Rev.* **1956**, *103*, 1127–1129.
18. Dementyev, A. E.; Cory, D. G.; Ramanathan, C. Dynamic Nuclear Polarization in Silicon Microparticles. *Phys. Rev. Lett.* **2008**, *100*, 127601.
19. Ladd, T. D.; Maryenko, D.; Yamamoto, Y.; Abe, E.; Itoh, K. M. Coherence Time of Decoupled Nuclear Spins in Silicon. *Phys. Rev. B* **2005**, *71*, 014401.
20. Schwartz, M. P.; Cunin, F.; Cheung, R. W.; Sailor, M. J. Chemical Modification of Silicon Surfaces for Biological Applications. *Phys. Status Solidi A* **2005**, *202*, 1380–1384.
21. Gupta, A. K.; Gupta, M. Synthesis and Surface Engineering of Iron Oxide Nanoparticles for Biomedical Applications. *Biomaterials* **2004**, *26*, 3995–4021.
22. Jiang, W.; Kim, B. Y. S.; Rutka, J. T.; Chan, W. C. W. Nanoparticle-Mediated Cellular Response Is Size-Dependent. *Nat. Nanotechnol.* **2008**, *3*, 145–150.

23. Nishi, Y. Study of Silicon−Silicon Dioxide Structure by Electron Spin Resonance I. *Jpn. J. Appl. Phys.* **1971**, *10*, 52–62.
24. Shen, T. D.; Koch, C. C.; McCormick, T. L.; Nemanich, R. J.; Huang, J. Y.; Huang, J. G. The Structure and Property Characteristics of Amorphous/Nanocrystalline Silicon Produced by Ball Milling. *J. Mater. Res.* **1995**, *10*, 139–148.
25. Zhao, L.; Mulkern, R.; Tseng, C. H.; Williamson, D.; Patz, S.; Kraft, R.; Walsworth, R. L.; Jolesza, F. A.; Albert, M. S. Gradient Echo Imaging Considerations for Hyperpolarized ^{129}Xe MR. *J. Magn. Reson., Ser. B* **1996**, *113*, 179–183.
26. Howarter, J. A.; Youngblood, J. P. Optimization of Silica Silanization by 3-Aminopropyltriethoxysilane. *Langmuir* **2006**, *22*, 11142–11147.
27. Jana, N. R.; Earhart, C.; Ying, J. Y. Synthesis of Water-Soluble and Functionalized Nanoparticles by Silica Coating. *Chem. Mater.* **2007**, *19*, 5074–5082.
28. Ferrari, M. Cancer Nanotechnology: Opportunities and Challenges. *Nat. Rev. Cancer* **2005**, *5*, 161–171.
29. Xu, H.; Yan, F.; Monson, E.; Kopelman, R. Room-Temperature Preparation and Characterization of Poly(ethylene glycol)-Coated Silica Nanoparticles for Biomedical Applications. *J. Biomed. Mater. Res.* **2003**, *66A*, 870–879.
30. Zhang, Z.; Berns, A. E.; Willbold, S.; Buitenhuis, J. Synthesis of Poly(ethylene glycol) (PEG)-Grafted Colloidal Silica Particles with Improved Stability in Aqueous Solvents. *J. Colloid Interface Sci.* **2007**, *310*, 446–455.
31. Cassidy, M. C., Atkins, T. M., Lee, M. Y., Kauzlarich, S. M., Marcus, C. M. To be submitted for publication.
32. Jain, R. K. Delivery of Molecular and Cellular Medicine to Solid Tumors. *Adv. Drug Delivery Rev.* **2001**, *46*, 149–168.
33. Li, D.; Dong, Y.; Ramos, R. G.; Murray, J. D.; MacLean, K.; Dementyev, A. E.; Barrett, S. E. Intrinsic Origin of Spin Echoes in Dipolar Solids Generated by Strong π Pulses. *Phys. Rev. B* **2008**, *77*, 214306.
34. Brown, C. Particle Size Distribution by Centrifugal Sedimentation. *J. Phys. Chem.* **1944**, *48*, 246–258.